The AIRS Forward Transmittance Model

L. Larrabee Strow, Scott Hannon, and W. Wallace McMillan
Physics Department
University of Maryland Baltimore County
1000 Hilltop Circle, Baltimore, MD, 21250

August 15, 1996

Contents

1 Introduction 2

2 Basic Radiative Transfer and the PolyChromatic Approximation 3

3 Spectroscopic Inputs 6
3.1 Spectroscopic Line Parameter Errors . . . 7
3.2 Molecular Line Shape Effects . . . 8
3.2.1 The CO_2 Line Shape . . . 9
3.2.2 Water Vapor Continuum . . . 10

4 Line-by-Line Calculations 11

5 k-Compressed Database 14

6 Fast Transmittance Model Parameters 15
6.1 Layering Grid . . . 16
6.2 Regression Profiles . . . 16
6.3 Breakout of Gases . . . 18
6.4 Predictors . . . 19
6.4.1 k_{fixed} . . . 20
6.4.2 k_{water} . . . 21
6.4.3 k_{ozone} . . . 21
6.4.4 k_{CO} . . . 22
6.4.5 $k_{methane}$ . . . 23
6.5 Regressions for Fast Transmittance Parameters . . . 24
6.6 Analytic Jacobians . . . 25

6.7 Summary of the Generation of the Forward Model 26

7 Sensitivity of the Forward Model to the AIRS Spectral Response Function 26

8 Validation of Forward Model and Fast Transmittance Algorithm 29

1 Introduction

Physical retrievals require an accurate "forward model" for radiative transfer relating atmospheric parameters to the observed channel radiances. In the context of this section the forward model is the relationship between atmospheric state parameters and associated layer transmittances, also termed a fast transmittance model. This model requires good knowledge of the molecular spectroscopy of the infrared active atmospheric constituents, and is especially demanding of spectral line shapes models. Outgoing atmospheric radiances contain emission lines at the higher altitudes with widths as small as 0.001 cm^{-1}. Performing radiative transfer at this spectral resolution, and then convolving the resultant radiances with the AIRS spectral response function would be many orders of magnitude too slow for EOSDIS. For this reason, the forward model must produce transmittances suitably convolved with the AIRS spectral response function so radiative transfer computations need only be performed for each AIRS channel.

The present forward model actually produces equivalent channel averaged absorption coefficients, k's, which are related to the layer transmittances, τ's, by $\tau = \exp(-k)$. For AIRS, a fast model for k is much more accurate than a model that directly returns layer τ's. The existing AIRS forward model lets H_2O, O_3, CH_4, and CO vary, as well as the temperature and local scan angle. All other gases are lumped into the "fixed gases" term. We also tentatively plan to let N_2O amounts vary. Note, although the observed radiances are sensitive to temperature via the Planck function, the temperature dependence of the transmittances is also important. Some variation in CO_2 amount will also be required, but this may be done "off-line" as a semi-continuous adjustment of the "fixed gas" transmittances. It may also be necessary to let some of the minor gases such as the CFC's vary as well. Transmittances are computed for each of the 100 atmospheric layers used for AIRS radiative transfer.

Over the years, a number of fast transmittance models have been developed for various satellite instruments[1, 2, 3, 4, 5, 6, 7, 8]. Some of these models have only been applied to the microwave region, which is easier to model since the measured radiances are essentially monochromatic. The present AIRS fast model most closely follows Susskind *et al.*[8] by parametrizing the absorption coefficients rather than transmittances. In addition, preliminary work has been performed with a new algorithm, OPTRAN, developed by McMillin *et al.*[5, 6]. Both the present AIRS algorithm and OPTRAN appear adequate for AIRS with similar cpu requirements[9].

The following sections discuss the essential components of an accurate AIRS forward model. These include (1) the radiative transfer equation and approximations used, (2) state-of-the-art molecular spectroscopy, (3) a line-by-line transmittance model that utilizes the best spectroscopic parameters and lineshapes, (4) a parametrized database of monochromatic absorption coefficients generated using the line-by-line transmittance model, (5) an empirical model to produce channel averaged transmittances as a function of the atmospheric state parameters, (6) a regression scheme to produce statistically accurate coefficients for this empirical transmittance model, (7) an accurate spectral response function for AIRS, and (8) proper validation of the AIRS forward model.

2 Basic Radiative Transfer and the PolyChromatic Approximation

The monochromatic radiance leaving the top of the atmosphere, excluding any scattering and surface reflection, is approximated by

$$R = \epsilon_s B\Big(T(s)\Big)\,\tau_{z,N} + \sum_{i=1}^{N} B\Big(T(i)\Big)\,\Big(\tau_{z,i-1} - \tau_{z,i}\Big), \tag{1}$$

where the atmospheric layers are numbered from space to the surface, 1 to N, respectively. $B\,(T\,(i))$ is the Planck function emission for layer i at temperature $T(i)$, $\tau_{z,i}$ is the layer-to-space transmittance from layer i to space, inclusive, and $T(s)$ and ϵ_s refer to the Earth's surface temperature and emissivity, respectively. For development of the AIRS forward model the polychromatic approximation is invoked, replacing the monochromatic layer-to-space transmittances with transmittances convolved with the AIRS spectral response function (SRF). If the convolved layer-to-space transmittances are used in the above equation the resulting radiances differ from convolved monochromatic radiances by $\leq$ 0.1 K in most cases. This difference is generally less than the nominal 0.2 K RMS noise of AIRS, and thus does not introduce any serious inaccuracies. The fast forward model produces effective *layer* transmittances since they can be modeled more accurately and because the AIRS retrieval algorithms perform radiative transfer based on layer transmittances. However, if polychromatic radiative transfer is performed using layer transmittances that have been directly convolved from the monochromatic layer transmittances, large radiance errors will result due to the breakdown of Beer's law. For this reason, the fast forward model is based on layer transmittances derived from ratios of convolved layer-to-space transmittances, thus preserving Beer's law to a much higher degree. Although an exponentiation is required to produce transmittances, this model provides for a relatively simple relationship between optical depths and atmospheric variables.

Figure 1 shows the great contrast between monochromatic brightness temperatures and AIRS observed brightness temperatures in a small portion of the 15 μm band of CO_2. This difference in resolution of the two spectra makes the development of the forward model quite complex. A simulated brightness temperature for clear sky conditions covering all the AIRS

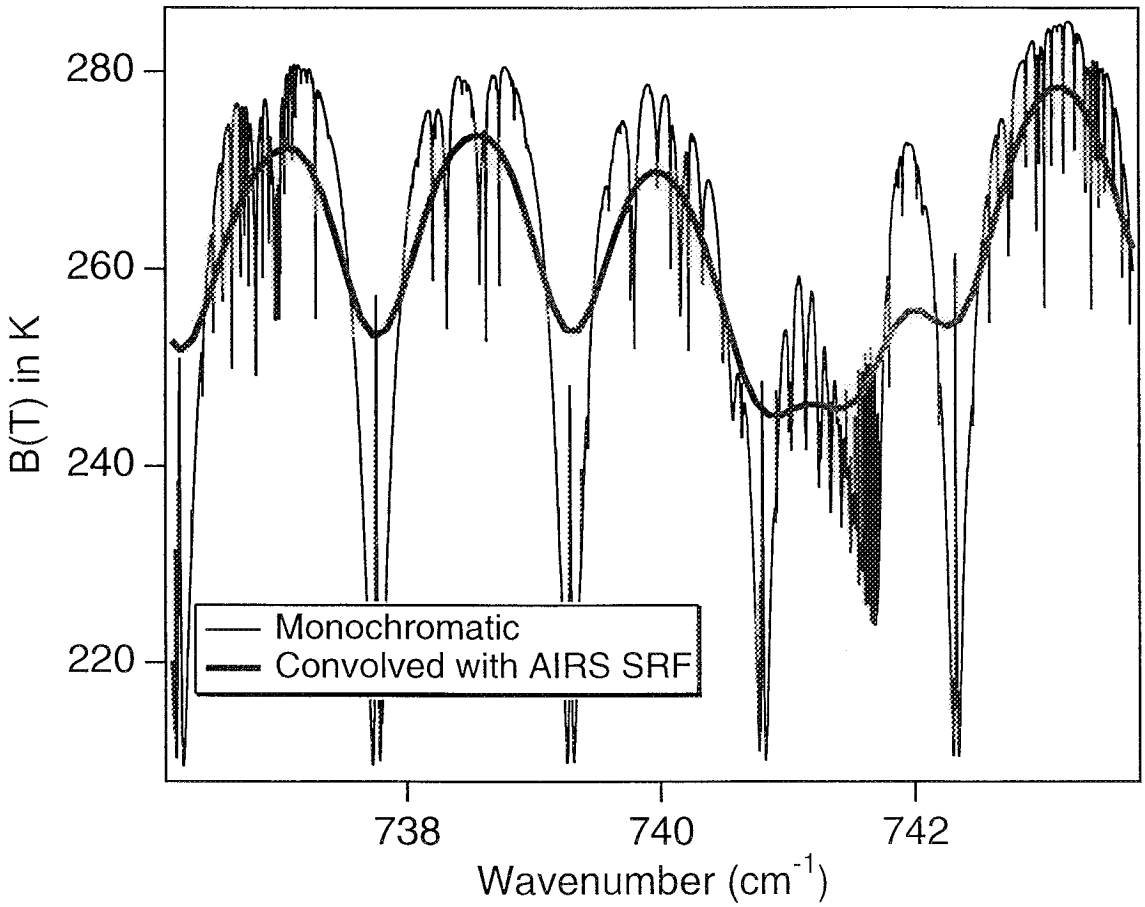

Figure 1: Comparison of monochromatic brightness temperatures to brightness temperatures convolved with the AIRS spectral response function.

channels, at the nominal AIRS spectral resolution, is shown in Fig. 2. The locations of the actual AIRS channels are shown in purple, the red channels will not be detected by AIRS.

Our fast transmittance model, which relates the profile variables to the layer optical depths, is called the Pressure Layer Optical Depth (PLOD) model because the optical depths are determined for layers of constant pressure. A simplified outline of how these effective layer transmittances are generated for the fixed gases in the atmosphere is:

1. Select a small set of atmospheric profiles that statistically spans the set of all possible observed atmospheric profiles. Currently, 36 profiles at 5 viewing angles are used for this

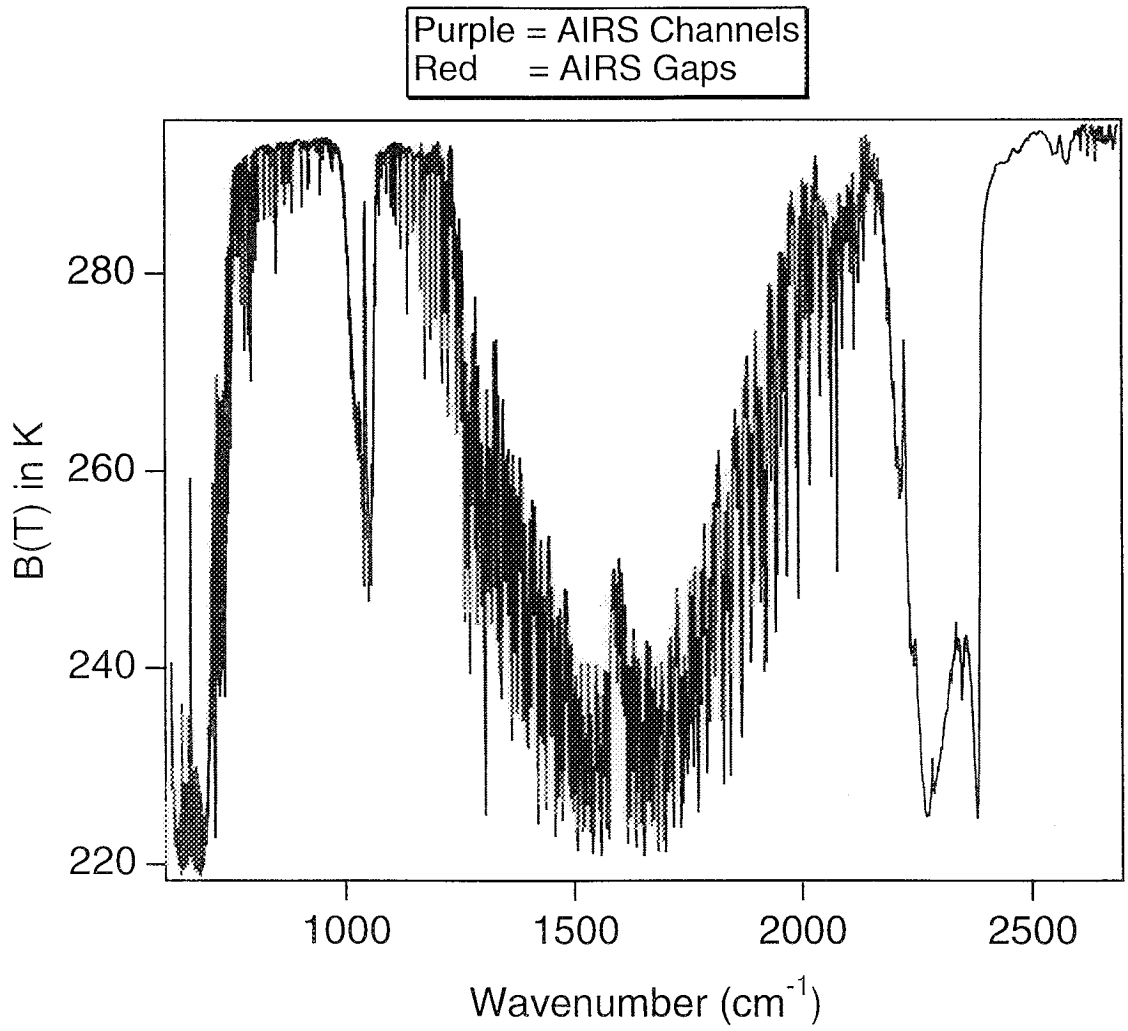

Figure 2: Simulated AIRS brightness temperature spectrum. Purple denotes AIRS channels, red denotes regions where AIRS does not have channels.

spanning set. More profiles or angles can be added as desired.

2. Generate monochromatic layer-to-space transmittances for all layers for these 36 profiles.
3. Convolve the layer-to-space profiles with the AIRS SRF.
4. Ratio the convolved layer-to-space transmittances to form effective layer transmittances,

$$\tau_{\text{eff}}(l) = \frac{\tau_{z,l}}{\tau_{z,l-1}}.$$

Note, $\tau_{z,l}$ is a convolved layer-to-space transmittance, and τ_{eff} is an effective (channel averaged) layer transmittance.

5. Take the natural log of these effective transmittances

$$k_{\text{eff}} = -\ln(\tau_{\text{eff}})$$

6. Fit the 36 * 5 k_{eff}'s for each layer to an empirical function,

$$k_{\text{eff}} = \sum_{i=1}^{n} c_i Q_i,$$

where Q_i is the i^{th} profile dependent predictor, n is the number of predictors, and the c_i are the so called fast transmittance coefficients that are determined from a least-squares fit.

The predictors are simple functions of parameters such as layer temperature, absorber amount, and viewing angle. However, because of the loss of Beer's law, some predictors involve profile parameters in layers above the layer of interest. Note, the regression is performed on $-\ln(\tau)$, the optical depth, and not τ itself as is done in many other fast transmittance models. A more detailed development of the fast model is given in Section 6. The generation of the monochromatic layer-to-space transmittances depends on accurate spectroscopy and a good line-by-line algorithm.

3 Spectroscopic Inputs

The ultimate goal is to produce a forward model that does not introduce significant errors in AIRS computed radiances. In the past, this has not been possible given the state-of-the-art in atmospheric spectroscopy. However, advances in laboratory measurements of line parameters, and advances in phenomenological spectral lineshape models make an accurate AIRS forward model a real possibility. This is especially important for H_2O. Radiosonde humidity errors,

coupled with always present errors in the time and space co-location of the radiosonde and AIRS measurements, make tuning of the AIRS H_2O radiances quite suspect. Consequently, the forward model is of fundamental importance for AIRS data products.

The sensitivity of the AIRS forward model to errors in spectroscopic line parameters and the development of improved spectral lineshape models for CO_2 and H_2O are summarized in the following subsections.

3.1 Spectroscopic Line Parameter Errors

Due to the dominance of either CO_2 or H_2O absorption in the majority of AIRS channels, the most important spectroscopy errors will generally be those associated with errors in the line parameters and line shapes of these two gases. The line center frequencies are well known, and thus should not be a noticeable source of error. Although there is a shift in line center frequency with pressure, these shifts are too small to be of concern for AIRS. The line parameters likely to introduce spectroscopy errors into the fast forward model for AIRS are the line strengths, line widths, and the temperature dependence of the line widths. In addition, errors in the water vapor continuum may also have an impact on the accuracy of the forward model.

Currently, the HITRAN92 [10] database is used for most atmospheric line parameters, supplemented by more recent H_2O linewidths measured by Toth[11, 12]. The AIRS forward model will be regularly updated with the latest available line parameters (HITRAN96, *etc.*). Because there are so many bands and molecules that contribute to the observed radiances, the accuracy of the existing line parameters is difficult to judge in detail. Fortunately for AIRS, many of the weaker lines of both CO_2 and H_2O have been measured in the laboratory .

In general the CO_2 line parameters are better known than those for H_2O. The line strengths for the stronger CO_2 lines are good to 3% or better, while the H_2O line strengths may only be good to 10%. The H_2O line strengths are also more likely to have different errors for different bands and isotopes. The effects of these potential errors in line strengths for CO_2 and H_2O are shown in Figures 3b and 4b, respectively. Note, these figures assume systematic errors in the line strengths and widths. While it is reasonable to expect some level of systematic error, at least over 20-50 cm^{-1}, there will also be random components to these errors.

The estimated uncertainty in the line widths are 10% for CO_2 and 20% for H_2O. Again, the H_2O widths are more likely to have both larger random and systematic errors between bands and isotopes. Line width errors will probably be the dominate source of spectroscopy errors for H_2O, while line strength and width errors will probably be of approximately equal importance for CO_2. The effects of these errors in line widths for CO_2 and H_2O are shown in Figures 3c and 4c, respectively.

The temperature dependence of the line widths is the least well known, with an uncertainty of perhaps 20% and sometimes more. However, of the four sources of errors discussed here it is the least important. A plot of the effects of a +20% error in the temperature dependence of the CO_2 line widths is shown in Figure 3d. The similar error for H_2O is much smaller than

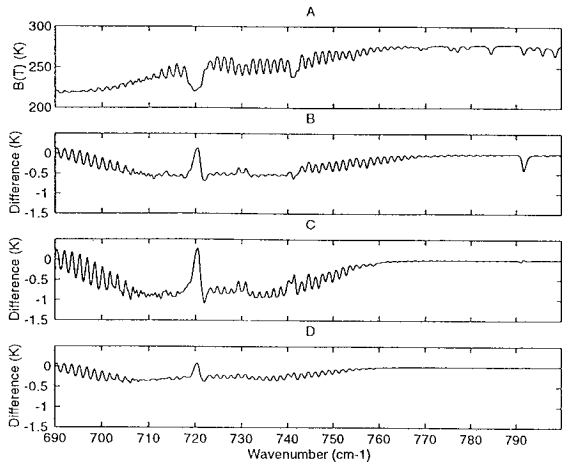

Figure 3: (a) A mean AIRS spectrum in a portion of the 15 μm CO_2 band. (b) The mean brightness temperature error due to a +5% error in CO_2 line strengths. (c) The mean brightness temperature error due to a +10% error in CO_2 line widths. (d) The mean brightness temperature error due to a +20% error in the CO_2 width temperature dependence.

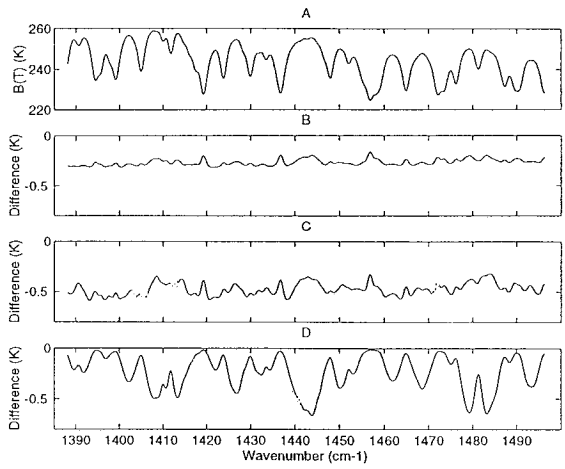

Figure 4: (a) A mean AIRS spectrum in a portion of the 7 μm H_2O band. (b) The mean brightness temperature error due to a +5% error in H_2O line strengths. (c) The mean brightness temperature error due to a +10% error in H_2O line widths. (d) The mean brightness temperature error due to a +25% error in the foreign broadened H_2O continuum.

those shown in Figures 4b and 4c.

The uncertainty in the H_2O foreign continuum may be as large as 25% in portions of the $7\mu m$ band. For AIRS, errors due to this peak in the 1400 cm^{-1} region. A plot of the impact of a +25% error in the H_2O foreign continuum is shown in Figure 4d. In other portions of the $7\mu m$ band these uncertainties are likely smaller.

All of the errors quoted here are somewhat conservative. Continuing laboratory spectroscopy efforts, especially in Europe, should lower the errors quoted here by a factor of two over the next several years.

3.2 Molecular Line Shape Effects

Much more problematic are errors in the spectral lineshapes of CO_2 and H_2O. Because of the large optical depths of CO_2 and H_2O in the atmosphere, their spectral line wings can be quite important, especially for remote sensing of temperature and humidity. For example, AIRS channels with the sharpest weighting functions are located in between lines or in the line wings where knowledge of the spectral line shape is very important. Moreover, it can be very

difficult to accurately measure line wing absorption in the laboratory because it is impractical to simulate atmospheric optical depths in a laboratory cell, especially for H_2O. It is also tedious and expensive to make these large optical depth measurements at the low temperatures found in the upper troposphere.

3.2.1 The CO_2 Line Shape

For CO_2, line mixing and duration-of-collision effects can dominate in many important temperature sounding channels in both the 4.3 μm and 15 μm regions. Strow *et al.* have made extensive studies of the CO_2 lineshape, both in the laboratory[13, 14, 15, 16], and using atmospheric observations [17, 18], that have been used in the development of a CO_2 lineshape appropriate for AIRS. Previous models for the important 4.3 μm CO_2 R-branch bandhead were inaccurate because they parametrized the sub-Lorentz absorption via either a line-mixing lineshape or a lineshape that allowed a finite duration-of-collision. A practical yet accurate model for this region that can be used in GENLN2 is under development by L. Strow and David Tobin [16]. This model explicitly includes both effects and models the laboratory data quite accurately. The 4.3 μm studies of CO_2 have also provided a duration-of-collision parameter that is directly applicable to the 15 μm CO_2 spectra, where this parameter is very hard to determine experimentally.

A recent laboratory study in the 700 cm^{-1} region of CO_2 [16] demonstrated that the existing CO_2 far-wing lineshapes[19] underestimate the absorption in between lines in this region. The same underestimate is also present in line-by-line calculations using the Cousin[19] lineshape when compared to validated HIS radiance measurements[20]. This underestimation results from using an empirical lineshape derived from 4.3 μm CO_2 spectra in the 15 μm calculations where this lineshape is no longer valid. The Cousin empirical lineshape tries to model both line-mixing and duration-of-collision effects using a parametrization only applicable to the far-wing duration-of-collision behavior. Because line-mixing is only about 1/2 as strong in the 15 μm region than the 4.3 μm region, the Cousin lineshape underestimates absorption in the wings of the strong CO_2 fundamental. (Line-mixing differences between the 4.3 μm and 15 μm bands are due to differences in the symmetries of these bands.) Using a new CO_2 lineshape model that treats line-mixing and duration-of-collision effects separately, both the laboratory spectra and HIS radiances can be modeled more accurately, without any adjustable parameters.

Q-branch line mixing lineshapes have been incorporated into GENLN2. However, the 4.3 and 15 μm combined P/R-branch line-mixing and far-wing duration-of-collision models have not yet been incorporated into GENLN2. We hope to update our version of GENLN2 with these new models in the future.

3.2.2 Water Vapor Continuum

Current line-by-line codes use the H_2O continuum developed by Clough *et al.*. This was originally based on the experimental measurements of Burch[21, 22, 23, 24] and subsequently modified due to inaccuracies uncovered by examining validated HIS measurements and the results of other field measurements. Although our current AIRS fast transmittance algorithm uses Clough's CKD 1.0 model, we have modified GENLN2 to use his latest model, CKD 2.1[25]. Numerous theoretical and experimental studies of the H_2O continuum in the wide infrared window regions exist because of their importance in sea and land remote sensing applications. Theoretical studies are especially important in these regions since laboratory measurements are extremely difficult due to insufficient optical depths in laboratory absorption cells. At the present time, we plan to use the latest CKD model in these window regions. Validation studies with AIRS in orbit may provide an opportunity to improve the water continuum in window regions.

Comparisons of validated HIS measurements inside the strong 6 μm H_2O band with line-by-line calculations using the CKD 2.1 continuum continue to exhibit large differences in brightness temperature (several K). There are several potential sources for these differences including co-location errors with radiosonde measurements of the temperature and humidity profile, H_2O lidar co-location errors, errors in H_2O spectroscopy, cloud contamination, and HIS instrument errors. Although Burch's measurements have been found to be quite accurate in the band wings, very little work has been performed to verify the in-band continuum where his measurements may be somewhat inaccurate due to the low spectral resolution. Consequently, Strow *et al.*[26, 16] recently made extensive laboratory measurements of the in-band H_2O continuum in order to verify and/or improve Burch's continuum and the CKD models in this important spectral region for AIRS humidity soundings.

These new laboratory measurements were used to derive the H_2O continuum between roughly 1350 and 2000 cm^{-1}. These results agree reasonably well with much of Burch's data, and with the CKD 2.1 continuum derived by Clough, *at Burch's reported wavenumber locations.* (Clough's definition of the continuum was used and comparisons to Burch's data are actually comparisons to a modification of Burch's data by Clough[27] to make it consistent with the CKD continuum definition). These new continuum values (both self- and foreign-broadened) do differ significantly from Burch's in the band center, by up to 100%. Comparisons with HIS validated spectra confirm the accuracy of this new continuum at the band center. See Fig. 6 for a comparison of validated HIS spectra and a line-by-line computation of the radiances using the new continuum values. Clearly, problems remain with higher altitude water emission, however we speculate that this may be due to inaccurate radiosonde measurements of humidity at pressure below several hundred mbar.

A significant result of these recent laboratory measurements is the realization that the experimental continuum values cannot be modeled accurately with a continuum that varies smoothly with wavenumber if Clough's definition of the continuum is used and the observing

instrument has a reasonably high spectral resolution, such as AIRS. This results from the rather strong super-Lorentz lineshape of H_2O close to the line centers. In Clough's model, any non-Lorentz behavior $\pm$ 25 cm^{-1} from the line centers is lumped into the continuum, as well as all absorption more than 25 cm^{-1} away from the line center. This gives a continuum with high frequency bumps near the line centers, and leads to inaccuracies if the continuum is modeled with a smooth curve, as in CKD 2.1. See Fig. 5 for an illustration of how bumpy the measured continuum is when a Lorentz lineshape is used to subtract the local absorption from the observed spectra. Clearly, a new formulation of the in-band H_2O continuum must be developed that puts the super-Lorentz lineshape into he so-called local part of the line-by-line calculation. This will effectively remove much of the high frequency structure in the remaining in-band continuum.

We are presently making extensive comparisons between validated HIS measurements inside the 6 μm H_2O band and line-by-line calculations using the CKD continuum and this new formulation of the water continuum. As stated earlier, these comparisons are difficult due to co-location problems and known errors in radiosonde humidity measurements that can be difficult to characterize. Given the importance of an accurate forward model for AIRS retrievals, we hope a future field campaign with the HIS instrument can be designed to give more definitive tests of our $H_2O$and CO_2 spectroscopy. We are especially concerned with persistent differences between HIS observations and calculations due to H_2O emission at pressures < 500 mbar. One possible field experiment to bring this problem to closure would be to fly both the HIS and a H_2O LIDAR on the ER-2 at the same time.

4 Line-by-Line Calculations

The monochromatic layer-to-space transmittances used to determine the parameters of the AIRS fast transmittance algorithm are indirectly generated from the GENLN2[28] line-by-line algorithm. Over the next several years, we will incorporate the spectroscopic advances discussed in the preceding section into GENLN2 in collaboration with David Edwards at NCAR (author of GENLN2).

GENLN2 is used indirectly to generate the layer-to-space monochromatic transmittances in the following sense. Currently 36 (or more) profiles are used in the regressions for the fast transmittance parameters. This would require 36+ line-by-line calculations for each of the 100 AIRS pressure layers. An examination of this requirement lead us to instead use GENLN2 to compute a very large look-up table of monochromatic absorption coefficients that could be interpolated to generate layer-to-space transmittances for any arbitrary atmospheric profile. This is possible because the monochromatic absorption coefficients generally vary quite slowly with temperature. Scaling for varying absorber amounts is trivial since monochromatic absorption coefficients are directly proportional to the absorber amount.

A look-up table with 11 evenly spaced temperatures is sufficient to accurately interpolate the

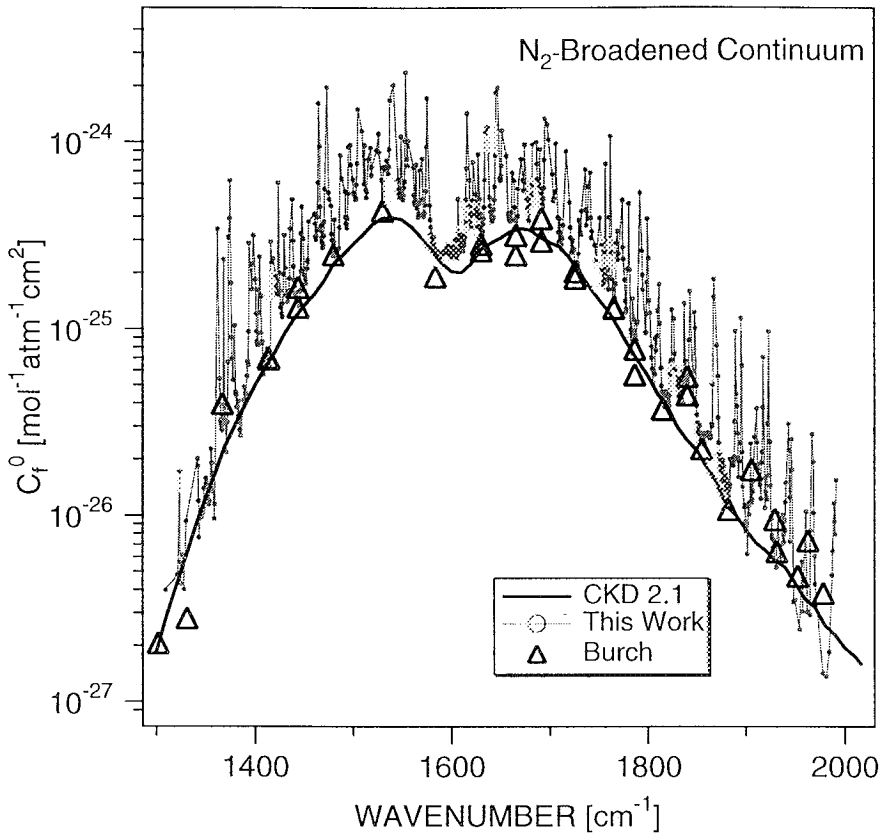

Figure 5: Recent measurements of the N_2-broadened continuum of H_2O taken at high spectral resolution[16] compared to previous measurements at low spectral resolution (Burch) and the CKD 2.1 continuum model of Clough[25].

layer absorption coefficients in temperature. This saves computational time since monochromatic layer absorption coefficients need only be calculated for 11 effective profiles rather than the 36+ profiles needed for generation of the fast transmittance algorithm parameters. The look-up table approach does introduces errors in water vapor transmittances since variations due to changes in the self-broadening of water are neglected. For AIRS, with channel widths varying from $\sim$ 0.5 to 2 cm^{-1}, this is a reasonably small error, generally $<$ 0.2K. However, due to its $\sim$ 35 Gbyte size, the look-up table is quite cumbersome to use.

This look-up table is composed of a large number of individual files. Each file, which we will call a **k** matrix, is 25 cm^{-1} long (point spacing of 0.0025 cm^{-1}or 10,000 points) by 100 pressure layers (0.015 to 1060 mbar). This pressure layer structure (see Fig. 7) was chosen

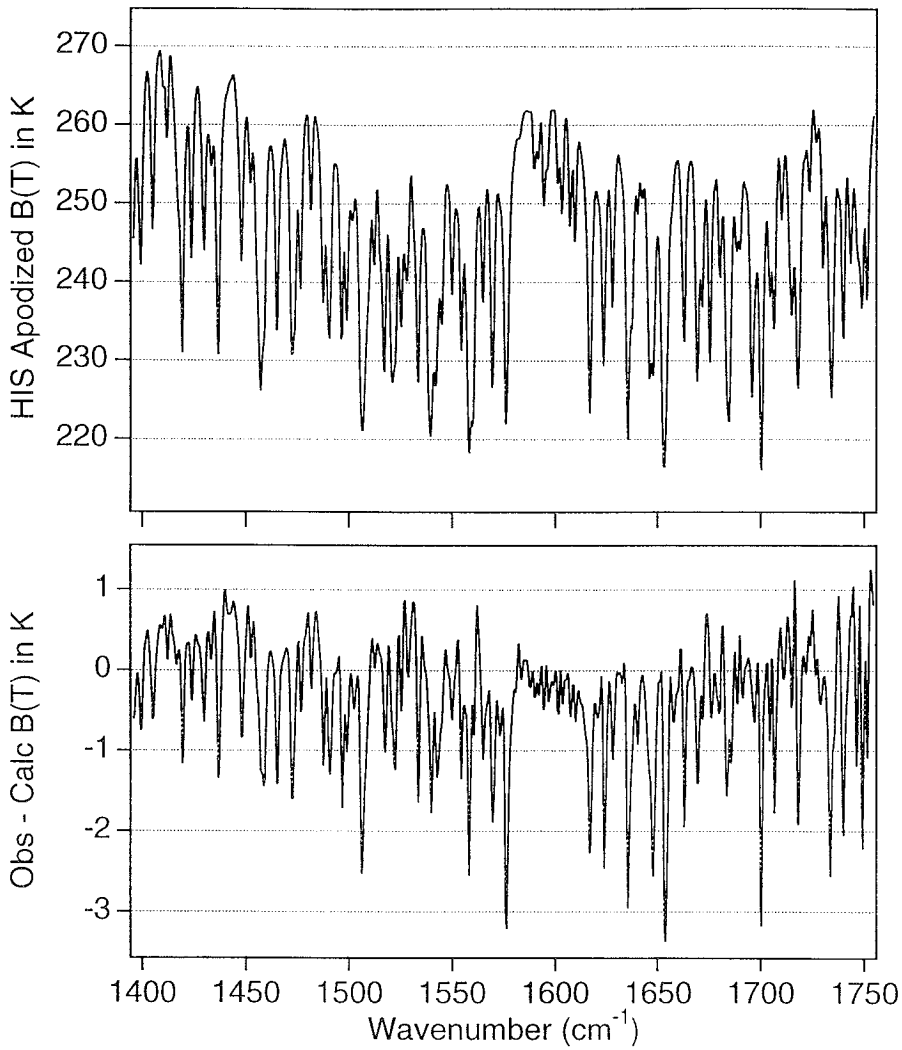

Figure 6: Apodized CAMEX1 validated HIS spectrum with differences between observed brightness temperatures and those calculated with our best H_2O continuum model. Note the good agreement at 1600 cm^{-1} where our new continuum model should be most accurate. This is also close to the temperature of the HIS low temperature calibration blackbody. Negative Obs-Calcs are believed to result from poor radiosonde humidity measurements at higher altitudes.

to produce errors below 0.2K in observed brightness temperatures for AIRS and is described in more detail later. For each gas and wavenumber region we compute 11 tables, which only differ by the temperature profile. These profiles are the U.S. Standard profile, and 10 profiles offset in ±10K increments from the U.S. Standard profile. The absorption coefficients are computed at a 0.0005 cm^{-1} grid and then averaged to the database grid spacing of 0.0025 cm^{-1}. Consequently the highest altitude absorption coefficients are not truly monochromatic, but have good integrated absorption coefficients. This produces negligible errors since the AIRS SRF is much wider than these high altitude lineshapes. Generally, 3 to 7 gases must be included per each 25 cm^{-1} region. Since absorption coefficients are stored rather than transmittances, variable gas amounts simply require multiplication by a scalar. Water continuum absorption is not included in these look-up tables since it is easy to compute separately. Gases that are included in HITRAN as cross-sections are not included in these tables since their absorption coefficients can also be computed quickly for any profile. These gases include the CFC's, and other minor constituents.

Absorption coefficients for all the HITRAN gases, except CO_2 and H_2O, are computed using the Voigt lineshape. As discussed earlier, the CO_2 and H_2O lineshapes are modified from the Voigt lineshape.

The effects of variable H_2O mixing ratio on H_2O linewidths can be included if required. Water is the only gas for which realistic variations in mixing ratio can affect linewidths. The current fast transmittance model does not include this effect. Also, GENLN2 does not currently include pressure shifts of line center frequency, although it could be modified to do so.

5 k-Compressed Database

We presently use the 35 Gbyte monochromatic database to generate the layer-to-space transmittances used in the determination of the fast transmittance model parameters. However, this database is cumbersome, difficult to manage and backup, and hard to transfer to the AIRS Project at JPL. Note, any significant changes in the AIRS spectral response function, including changes in the channel center wavenumber, will require generation of a new AIRS fast forward model. Although this is an "off-line" computation, it can be automated so the AIRS processing is not unduly delayed if the SRF changes. In addition, any improvements to the spectroscopy will require replacement of the relevant portions of the 35 Gbyte look-up table. For example, once AIRS has stabilized after launch, the actual center wavenumber of each channel will be determined. We expect these channel centers to shift very little about their mean, allowing interpolation of the observed radiances to a fixed grid of channel centers. Once the mean channel centers are determined, the associated fast transmittance parameters for these channels will be computed and used in the retrievals.

In order to avoid use of either the cumbersome 35 Gbytes monochromatic database or a slow line-by-line code, we have developed a compressed version of the monochromatic database that

is easy to use, fast, and portable. This compressed database, which we call the "k-Compressed Database" was described in detail in a recent publication[29], and is only summarized here. This database and the codes to generate the AIRS forward model parameters will be installed at JPL so a new forward model can be generated anytime the AIRS SRF or channel centers change significantly.

The k-Compressed Database is essentially a singular value decomposition of the monochromatic database. Since there is great redundancy in the monochromatic database the singular value decomposition can be heavily truncated. The k-Compressed database includes a compact representation of the monochromatic database, $\hat{\mathbf{k}}$, given by

$$\hat{\mathbf{k}} \approx \mathbf{U}^T \mathbf{k}_{10,000\,\nu\text{'s by }100\text{ x }11\text{ layers}} = \Sigma \mathbf{V}^T, \tag{2}$$

and the associated matrix $\mathbf{U}$, which form an orthogonal basis set for the absorption coefficients stored in the monochromatic database. Note, $\mathbf{U}$, Σ, and $\mathbf{V}^T$ are all the *truncated versions* of these quantities. The SVD is done with a Lanczos bidiagonalization algorithm (with reorthogonalization) which sequentially finds the largest to smallest singular values and vectors. The level of truncation for each 25 cm^{-1} table for each gas is primarily determined by testing the effects of truncation on calculated AIRS brightness temperatures. Final determination of the size of the k-Compressed database is still underway, but it will be significantly smaller than 600 Mbytes. Because of the large dynamic range of the CO_2 and H_2O absorption coefficients, we actually compress the $k^{1/4}$ instead of k for these two gases.

The reconstructed $\mathbf{k}$ matrix (or monochromatic database table) is easily computed by matrix multiplication,

$$\mathbf{k}_{10,000\,\nu\text{'s by }100\text{ x }11\text{ layers}} = \mathbf{U}\hat{\mathbf{k}}. \tag{3}$$

If we rearrange the $\hat{\mathbf{k}}$ elements into 100 layers by 11 temperatures for each different basis set vector we find the very nice property that they vary smoothly with both layer, and more importantly, with temperature. This means that if we want a $\mathbf{k}$ for a particular temperature profile we can interpolate the compressed absorption coefficients, $\hat{\mathbf{k}}$'s, in temperature instead of interpolating all 10,000 points in wavenumber space.

We have also generated k-Compressed tables to enable interpolation for the effects of variable self-broadening in H_2O, if ultimately needed for AIRS. This can be done with the standard monochromatic database, but it would increase its size and make it harder to use.

This database may also prove quite useful for various radiative transfer studies using AIRS. In addition, it can be used by other instruments (such as MODIS) for generation of their forward model parameterizations.

6 Fast Transmittance Model Parameters

All the steps needed to generate accurate layer-to-space monochromatic transmittances have been described. These are the main inputs to the regressions that determine the fast trans-

mittance parameters. Before describing the fast model in detail, the AIRS pressure layer grid is presented followed by a discussion of the profiles used in the regression for the fast model parameters.

6.1 Layering Grid

The atmospheric pressure layer grid was selected to keep radiative transfer errors well below the instrument noise. Grid characteristics are a factor of the spectral region(s) of observation, the instrument resolution, and instrument noise. The speed of the final fast transmittance model will depend on the number of layers, so excessive layering should be avoided.

Simulations using GENLN2 indicate that some channels need a top layer with pressures as small as 0.01 mbar, an altitude of $\sim$ 80 km. The region of primary importance to AIRS is the troposphere and lower stratosphere, where layers on the order of 1/3 of the nominal 1 km vertical resolution of AIRS retrievals are desired. Smoothly varying layers facilitate interpolation and avoid large changes in layer effective transmittances. The following relation defines the pressures layers selected for AIRS,

$$P(i) = \left(a\, i^2 + b\, i + c\right)^{7/2} \tag{4}$$

where P is the pressure in mb; i is the layer boundary index and ranges from 1 to 101; and the parameters a, b, and c were determined by solving this equation for $P(1) = 1100$ mb, $P(38) = 300$ mb, and $P(101) = 5 \times 10^{-3}$ mb. The 101 pressure layer grid points in turn define the 100 AIRS layers. These layers vary smoothly in thickness from several tenths of a kilometer near the surface to several kilometers at the highest altitudes. Figure 7 shows a plot of this atmospheric layer structure.

6.2 Regression Profiles

One other necessary pre-processing step is the selection of a set of profiles for calculation of the layer-to-space transmittances. The transmittances for these profiles become the regression data for the fast transmittance coefficients. These profiles should span the range of atmospheric variation, but on the whole, should be weighted towards the more typical cases. The range of variation provides the regression with data points covering the range of behaviors, while the weighting of the mix of profiles towards more typical cases produces a transmittance model that works best on more statistically common profiles.

The process of calculating and convolving monochromatic layer-to-space transmittances is generally computationally intensive, thus imposing a practical limit on the number of profiles one can calculate for use in the regression. As discussed earlier, 36 regression profiles (at 5 viewing angles each) are sufficient to cover most of the profile behavior. This number is a compromise between the available time and computing resources and the estimated needs for

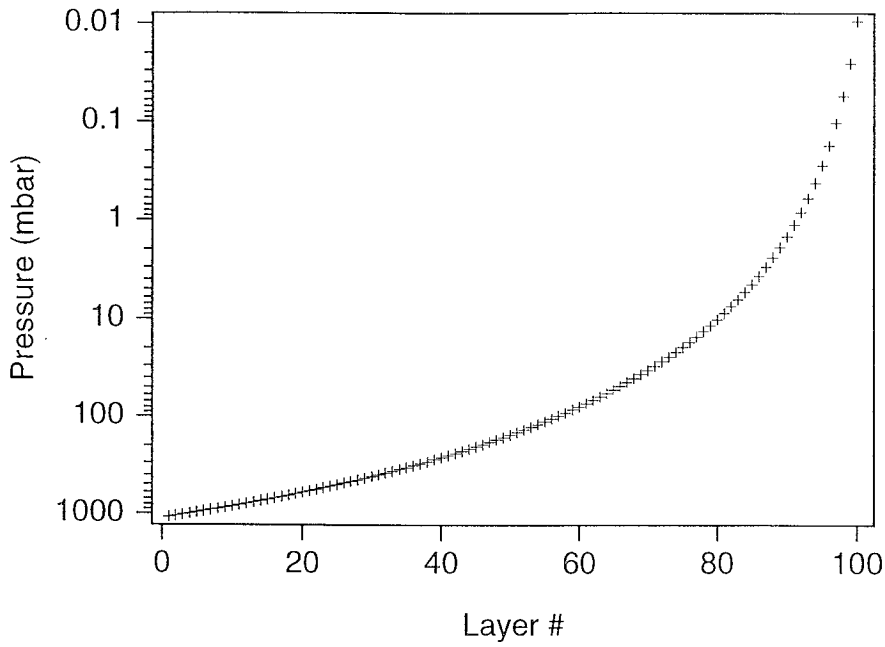

Figure 7: Our recent measurement of the N_2-broadened continuum of H_2O taken at high spectral resolution.

spanning the range of profile behavior in the regression. Choosing too few profiles leads to accuracy problems for profiles outside the range of behaviors considered. Choosing more profiles than necessary does not hurt the fast model, but does consume extra time and computer resources in the creation of the model.

Each profile should cover the necessary pressure (altitude) range with data for temperature as well as absorber amount for each of the gases allowed to vary. The fixed gases include all those whose spatial and temporal concentration variations have a negligible impact on the observed radiances. For AIRS, the variable gases include H_2O, O_3, CO, CH_4, and N_2O. At present, we have developed transmittance models for H_2O, O_3, CO, and CH_4; all other gases are in the "fixed gas" category. In the future we will also let N_2O vary and possibly CO_2. We have not yet decided how to handle slowly increasing CO_2 levels in the forward model.

For those satellite viewing angles relevant to the AIRS instrument (0 to 49 degrees), the effects of viewing angle can be fairly well approximated by multiplying the nadir absorption coefficient by the secant of the local path angle (there is a somewhat minor refractive effect at large angles which this ignores). We use five local viewing angles: 0, 38, 49, 56, and 63 degrees, which cover the complete 0-49 degree satellite view angle range.

6.3 Breakout of Gases

With the layering grid and regression profiles selected, the monochromatic layer-to-space transmittance may be calculated. The gases are distributed into sub-groups as follows:

$$\begin{aligned} & F \\ & F + V_1 \\ & F + V_1 + V_2 \\ & \quad \cdots \\ & F + V_1 + V_2 + \ldots + V_n \end{aligned} \tag{5}$$

where F refers to the fixed gases, and V_j to the j^{th} variable gas. Such a grouping reduces the errors inherent in separating the gas transmittances after the convolution with the instrument spectral response function. The convolution of a product of terms is in general not the same as the sum of the terms convolved individually. However, if we make use of the above form, the effective layer-to-space transmittance of the j^{th} variable gas by itself is

$$\tau_{z\,\mathrm{eff}}(V_j) = \frac{\tau_z(F + V_1 + V_2 + \cdots + V_{j-1} + V_j)}{\tau_z(F + V_1 + V_2 + \cdots + V_{j-1})} \tag{6}$$

and the total transmittance of all the individual gases together is

$$\tau_{z\,\mathrm{total}} = \tau_{z\,\mathrm{eff}}(F) \times \prod_{j=1}^{n} \tau_{z\,\mathrm{eff}}(V_j) \tag{7}$$

Thus, all the terms except $\tau_z(F + V_1 + V_2 + \cdots V_n)$ cancel, leaving only the correct, convolved transmittance for all gases combined. Generally, the order in which the variable gases are added after the fixed gases should be in order of increasing importance to the total transmittance. This depends upon the spectral region and particulars of the instrument, as well as the range of variation of gas amounts.

The following discussion in this subsection assumes only three categories of gases; fixed, H_2O, and O_3, for the sake of simplicity. The monochromatic layer-to-space transmittances are calculated and grouped into three sets

$$\begin{aligned} F &= \tau_z(\text{fixed}) \\ FW &= \tau_z(\text{fixed} + \text{water}) \\ FWO &= \tau_z(\text{fixed} + \text{water} + \text{ozone}) \end{aligned} \tag{8}$$

and then convolved with the AIRS spectral response function. Water continuum absorption is excluded above since it varies slowly with wavenumber and does not need to be convolved with

the AIRS instrument function. The water continuum is added to the total transmittance as a separate term later.

For each layer l, the convolved layer-to-space transmittances are ratioed with transmittances in the layer above, $l-1$, to form effective layer transmittances for fixed (F), water (W), and ozone (O)

$$\begin{aligned} F_{\text{eff}}(l) &= \frac{F(l)}{F(l-1)} \\ W_{\text{eff}}(l) &= \frac{FW(l)}{FW(l-1)} \div \frac{F(l)}{F(l-1)} \\ O_{\text{eff}}(l) &= \frac{FWO(l)}{FWO(l-1)} \div \frac{FW(l)}{FW(l-1)} \end{aligned} \tag{9}$$

The zeroth layer transmittance (*i.e.* when $l-1=0$) is taken to be exactly 1.0. The negative logarithm of these layer effective transmittances is taken to get effective layer optical depths,

$$\begin{aligned} k_{\text{fixed}} &= -\ln(F_{\text{eff}}) \\ k_{\text{water}} &= -\ln(W_{\text{eff}}) \\ k_{\text{ozone}} &= -\ln(O_{\text{eff}}). \end{aligned} \tag{10}$$

6.4 Predictors

These effective layer optical depths become the dependent variables in a regression to calculate the fast transmittance coefficients that relate a set of profile dependent predictors to the layer effective optical depth. It is important that some care be used to restrict the regression to k values that are significant for radiative transfer.

The optimal set of predictors used to parameterize the effective layer optical depth depends upon the gas, the order in which they are separated out, the instrument's spectral response function, the range of viewing angle, the spectral region, and even the layer thicknesses. In short, no one set of predictors is likely to work well in every case. Finding the set of predictors which gives the best results is in part a matter of trial and error. However, there are some general trends. For example, Fig. 8 illustrates a representative variation of optical depth with temperature. The variable viewing angle primarily imparts an offset as well as a small change in slope to the curve. Fig. 9 shows a fairly well behaved variation of optical depth with water amount, while Fig. 10 shows a behavior that is more difficult to model. Note, Figs. 9 and 10 are for the *same* channel, but different layers!

For an instrument such as AIRS with thousands of channels, it is difficult to develop individual optimal predictors for each channel. At this point we have developed one set of predictors that works sufficiently well for all channels. This set of predictors was determined by extensive trial and error testing of a few representative channels estimated to span the range of behaviors

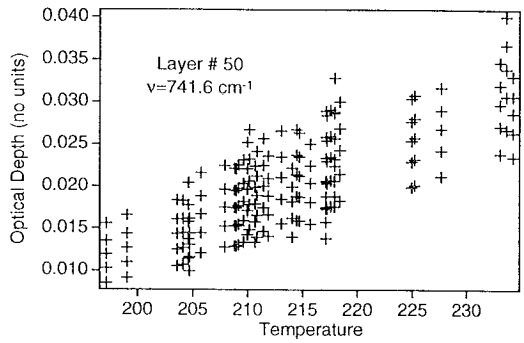

Figure 8: Example of how the PLOD k_{fixed} varies with layer temperature. The vertical stacks of points are variations in the AIRS viewing angle.

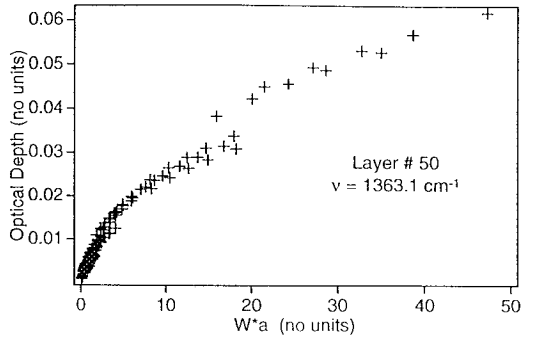

Figure 9: Example of how the PLOD k_{water} varies with $W * a$ (see text for definitions).

present in the entire channel set. The most difficult channels to model appear to be ones with low altitude water lines and those covering the strong ozone band.

The regression is prone to numerical instabilities if the values of the predictors vary too greatly. Consequently, we follow the usual practice of defining the predictors with respect to the values of a reference profile, either by taking a ratio or an offset. There is also a danger of numerical instability in the results of the regression due to the interaction of some of the predictors. Sensitivity of the output to small perturbations in the predictors is avoided by systematic testing. There are practical difficulties in detecting small problems since we are performing on the order of 1 million regressions. We hope to regularize these regressions in the future in a way that might allow automatic trimming of unnecessary predictors on a channel by channel basis.

6.4.1 $\mathbf{k}_{\text{fixed}}$

The following terms appear to be the best predictors for the fixed gases:

$$\begin{array}{ccc} 1)\, a & 2)\, a^2 & 3)\, a\, T_r \\ 4)\, a\, T_r^2 & 5)\, T_r & 6)\, T_r^2 \\ 7)\, a\, T_z & 8)\, a\, T_z / T_r & \end{array} \tag{11}$$

where a is the secant of the local path angle, T_r is the temperature ratio $T_{\text{profile}}/T_{\text{reference}}$, and T_z is the pressure weighted temperature ratio above the layer

$$T_z(l) = \sum_{i=2}^{l} P(i) \left(P(i) - P(i-1) \right) T_r(i-1) \tag{12}$$

where $P(i)$ is the average layer pressure for layer i.

6.4.2 k_{water}

The water algorithm is broken into two parts; one where the total water optical depth above the current layer is less than 5, denoted as profiles with $kz_{\text{water}} \leq 5$, and another for regions with profiles where $kz_{\text{water}} > 5$. For $kz_{\text{water}} \leq 5$ the best predictors for k_{water} were determined to be:

$$\begin{array}{ccc} 1)\, W\,a & 2)\, \sqrt{W\,a} & 3)\, W\,a\,dT \\ 4)\, (W\,a)^2 & 5)\, W\,a\,dT\ |\,dT\,| & 6)\, (W\,a)^3 \\ 7)\, W_z\,a & 8)\, \sqrt{W\,a}\,dT & 9)\, \sqrt[4]{W\,a} \\ 10)\, (W_z\,a)^2 & 11)\, \sqrt{W_z\,a} & \end{array} \tag{13}$$

and for $kz_{\text{water}} > 5$ we use

$$1)\, W\,a \quad 2)\, (W\,a)/(W_z\,a)^2 \tag{14}$$

where W is the water amount ratio $W_{\text{profile}}/W_{\text{reference}}$, dT is the temperature offset $T_{\text{profile}} - T_{\text{reference}}$, and W_z is the pressure weighted water amount above ratio, given by,

$$W_z(l) = \frac{\sum_{i=1}^{l} P(i)(P(i) - P(i-1))W_{\text{profile}}(i)}{\sum_{i=1}^{l} P(i)(P(i) - P(i-1))W_{\text{reference}}(i)} \tag{15}$$

where $P(i)$ is the layer pressure for layer i and $P(0) = 2\,P(1) - P(2)$.

Unfortunately, this results in the need to maintain a running sum of the water optical depth as one loops down over the layers. The root of this problem is the occurrence in many strong water channels of an abrupt change in the functional dependence of the water predictors at total optical depths of 3-5. An example of this can be seen in Fig. 10, where there is a drastic change in the behavior of the optical depths for $W * a$ in the range of 2-5. We were spared similar problems with fixed gases because the only absorber amount variation comes from a variation in the secant of the local path angle.

Since the water continuum is not included above, the effective layer optical depth for water only includes the near wing portion of the water line absorption; the far wing portion is added in separately before taking the exponential to obtain a layer transmittance. (The continuum absorption coefficients can be computed very quickly.)

6.4.3 k_{ozone}

The best predictors for ozone were determined to be:

$$1)\, O\,a \quad 2)\, \sqrt{O\,a} \quad 3)\, O\,a\,dT$$

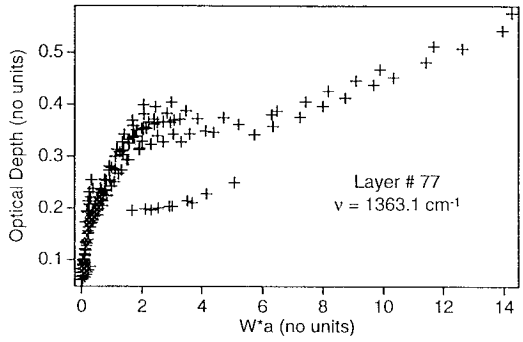

Figure 10: Example of how the variation of PLOD k_{water} with $W * a$ can change abruptly.

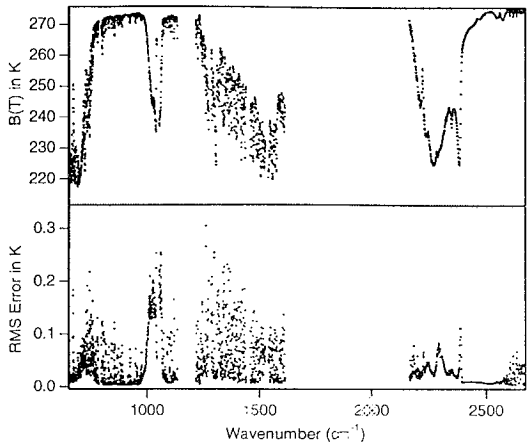

Figure 11: RMS fitting errors of the PLOD model for AIRS.

$$\begin{array}{ccc} 4)\ (O\,a)^2 & 5)\ \sqrt{O\,a}\,dT & 6)\ O_z\,a \\ 7)\ O\,a\sqrt{O_z\,a} & 8)\ O\,a\,W\,a & 9)\ TO_z\,O\,a \end{array} \tag{16}$$

where W is the water amount ratio $W_{\text{profile}}/W_{\text{reference}}$, O is the ozone amount ratio $O_{\text{profile}}/O_{\text{reference}}$, O_z is the pressure weighted ozone amount ratio above

$$O_z(l) = \sum_{i=2}^{l} P(i)\Big(P(i) - P(i-1)\Big)\,O(i-1) \tag{17}$$

and TO_z is the pressure and ozone weighted temperature ratio above

$$TO_z(l) = \sum_{i=2}^{l} P(i)\,\Big(P(i) - P(i-1)\Big)\,T_r(i-1)O(i-1) \tag{18}$$

6.4.4 $\mathbf{k_{CO}}$

The best predictors for carbon monoxide (CO) were determined to be:

$$\begin{array}{ccc} 1)\ C\,a & 2)\ \sqrt{C\,a} & 3)\ C\,a\,dT \\ 4)\ \sqrt[4]{C\,a} & 5)\ \sqrt{C\,a}\,dT & 6)\ C_z\,a \\ 7)\ \sqrt{C_z\,a} & 8)\ \sqrt[4]{C_z\,a} & \end{array} \tag{19}$$

where a and dT are as previously defined, and C and C_z are as defined for W and W_z, respectively, in the $\mathbf{k}_{water}$ subsection except for CO. Predictor (8) is likely to change as the algorithm is further refined. The terms for fixed, water, and ozone are unchanged, but could be better optimized for this spectral region.

6.4.5 $\mathbf{k}_{\text{methane}}$

The best predictors for methane were determined to be:

$$\begin{array}{ccc} 1)\, M\,a & 2)\, \sqrt{M\,a} & 3)\, M\,a\,dT \\ 4)\, (M\,a)^2 & 5)\, M_z\,a & \\ 6)\, M\,a\,TM_z & 7)\, \sqrt{M_z\,a} & \end{array} \tag{20}$$

where a and dT are as previously defined, M and M_z are as defined for W and W_z, respectively, in the $\mathbf{k}_{water}$ subsection except for methane, and TM_z is defined as for TO_z in the $\mathbf{k}_{\text{ozone}}$ subsection except for methane.

Since there is essentially no ozone absorption in the methane spectral region there are no ozone terms. The terms for fixed gases and water *in the region where separate terms for methane are included* are modified as follows:

Fixed gas predictors (mostly N_2O parameters):

$$\begin{array}{ccc} 1)\, a & 2)\, a^2 & 3)\, T_r \\ 4)\, a\,T_r & 5)\, (a\,T_r)^2 & 6)\, a\,T_z \end{array} \tag{21}$$

where a, T_r, and T_z are as previously defined in the $\mathbf{k}_{\text{fixed}}$ subsection.

Water predictors: For $kz_{\text{water}} \leq 5$ we use

$$\begin{array}{ccc} 1)\, W\,a & 2)\, W_z\,a & 3)\, \sqrt{W\,a} \\ 4)\, (W\,a)^2 & 5)\, W\,a\,dT & 6)\, (W\,a)/(W_z\,a) \\ 7)\, (W\,a)/(\sqrt{W_z\,a}) & 8)\, dT\,\sqrt{W\,a} & 9)\, W\,a\,C_z\,a \\ 10)\, (\sqrt{W\,a})/(W_z\,a) & 11)\, (W\,a)^3 & \end{array} \tag{22}$$

and for $kz_{\text{water}} > 5$ we use

$$1)\, W\,a \quad 2)\, (W\,a)/(W_z\,a)^2 \tag{23}$$

where the various parameters are as defined in the preceding subsections.

The CO fast model fitting errors are very low, better than 0.1K. The larger errors in the CO spectral region are due to H_2O. CH_4 fitting errors are higher, on the order of 0.2K. However it is difficult to completely separate H_2O and CH_4 contributions to the spectrum so we cannot completely separate errors due to these two gases where CH_4 emission is significant.

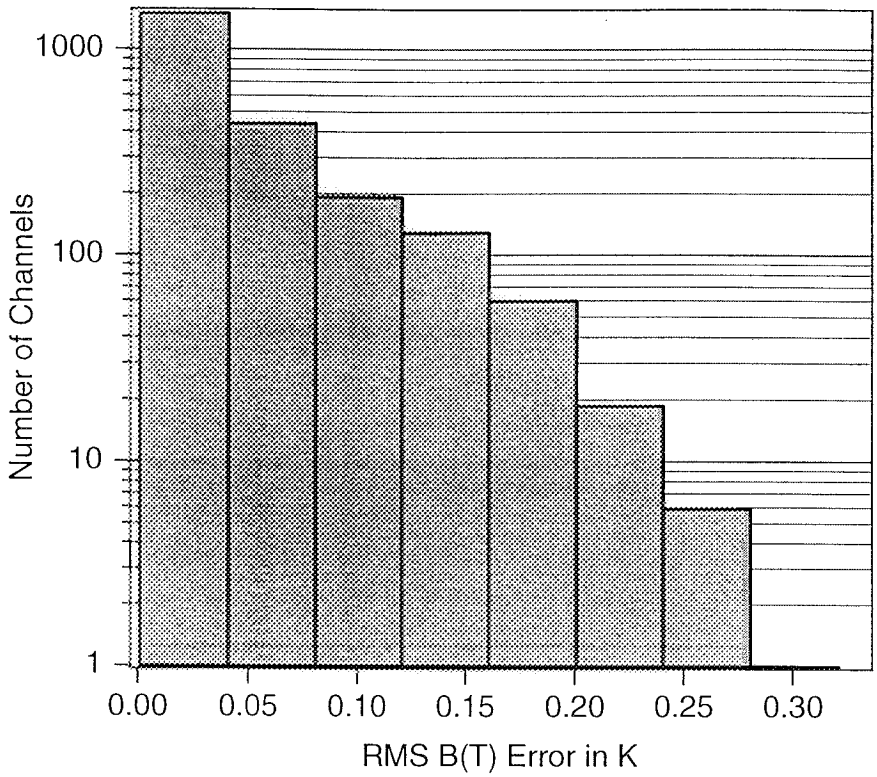

Figure 12: Histogram of the fast model fitting errors for all channels.

6.5 Regressions for Fast Transmittance Parameters

The accuracy of radiative transfer calculations made with the PLOD fast transmittances improve significantly if the data is weighted prior to performing the regression. Radiative transfer is insensitive to layers for which the change in layer-to-space transmittance across the layer is ~ zero. This occurs when either the layer effective transmittance is ~ unity, or when the layer-to-space transmittance above the layer is ~ zero. Therefore, the data going into the regression is not all of equal importance to the final accuracy of radiative transfer calculations made with the model. We found it useful to weight the data in terms of both its effective layer optical depth as well as the total optical depth of all the layers above the layer under consideration.

The spectral dependence of the fitting errors are shown in Fig. 11 and a histogram of these errors in Fig. 12. The errors are calculated with respect to the regression profile set, comparing the input data with the PLOD model calculated values. Errors calculated for a large independent profile set were very similar and are shown in Figs. 13 and 14. In general the RMS errors are

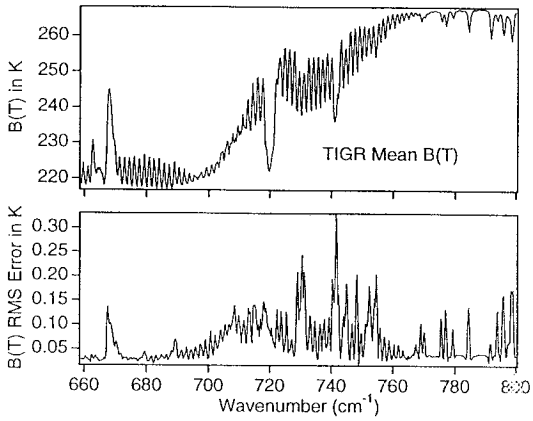

Figure 13: Forward model RMS errors over the 1200 TIGR profiles in the 15 μm temperature sounding region.

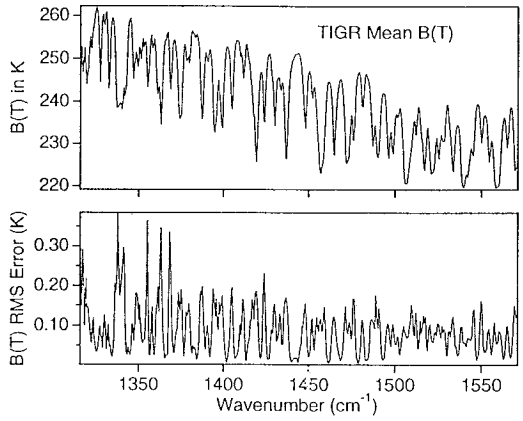

Figure 14: Forward model RMS errors over the 1200 TIGR profiles in a region sensing tropospheric H_2O.

at or below the estimated signal noise and spectroscopic errors. As previously mentioned, the largest errors are generally associated with either low altitude water or are inside the strong ozone band near 1100 cm^{-1}.

6.6 Analytic Jacobians

Significant savings in computer time may be possible if analytic Jacobians, $\partial R/\partial Q$ where R is the radiance and Q is an atmospheric variable, can be used instead of finite difference Jacobians. Currently, this option is under investigation. Preliminary work indicates the analytic derivatives of the PLOD fast model compare quite well with finite difference Jacobians. However, the analytic Jacobians are still relatively slow because of the dependence of the transmittances on profile variables above the layer under consideration. This is illustrated by the temperature Jacobian for arbitrary layer L,

$$\frac{\partial R}{\partial T(L)} = \epsilon_s B(T_s)\frac{\partial \tau_{z,N}}{\partial T(L)} + \frac{\partial B(L)}{\partial T(L)}\left(\tau_{z,L-1} - \tau_{z,L}\right) - B(L)\frac{\partial \tau_{z,L}}{\partial T_L} + \sum_{l=L+1}^{N} B(l)\left(\frac{\partial \tau_{z,l-1}}{\partial T(L)} - \frac{\partial \tau_{z,l}}{\partial T(L)}\right). \tag{24}$$

The τ's above are all layer-to-space transmittances, $T(L)$ is the temperature of layer L, B is the Planck function, T_s is surface temperature and ϵ_s is the surface emissivity. The sum from $l = L + 1$ to N in this expression is time consuming, and non-physical for the monochromatic case. This term should be relatively small, and we hope to develop a fast approximation for it that avoids the time consuming sum over layers.

6.7 Summary of the Generation of the Forward Model

The steps involved in generating the fast forward model for AIRS are summarized in the flowchart shown in Fig. 15.

7 Sensitivity of the Forward Model to the AIRS Spectral Response Function

Simulations using the AIRS SRF and monochromatic radiance spectra were performed to investigate the sensitivity of AIRS spectra to the spectral response function (SRF). These tests evaluated both the effects of the estimated uncertainties in the SRF, as well as the sensitivity of the convolved spectra to the far wings of the SRF. The latter subject has implications for the off-line computational needs for creating the fast forward model.

Each AIRS channel possesses a slightly different SRF, varying in both the shape of the SRF, particularly the far wing, and the resolution. Potential sources of error result from uncertainties in the resolution, channel center frequency, and SRF shape. The estimated uncertainty in resolution is ~ 2% or better, and for channel center frequency ~ 1% or better. The SRF shape may only be measured to approximately the 10^{-3} level. Figures 16b, 17b, and 18b illustrate the brightness temperature errors resulting from a 2% error in resolution at 15, 7, and 4 μm, respectively. Similarly, figures 19, 20, and 21 illustrate the brightness temperature errors resulting from a 1% shift in the channel center frequencies at 15, 7, and 4μm, respectively.

Figure 22 shows the latest estimates for the AIRS SRF. The magnitude of the wing intensity varies with spectral region and detector array, with the probable range in the SRF's illustrated in Figure 22. The gradually decreasing wings of the AIRS SRF's require convolution over many halfwidths if forward model convolution errors $\leq$ 0.2K (AIRS rms noise level) are desired. This presupposes the AIRS SRF can be measured before launch to an accuracy on the order of 10^{-4}.The requirement to convolve a large spectral range impacts on the off-line computational resources necessary to recompute the AIRS forward model, but will not seriously impact AIRS operational data processing.

The impacts of the variation in AIRS SRF and the number of halfwidths required to limit the error due to convolution are shown in Figures 23b and c, and 24b and c at 15 and 4 μm, respectively. As illustrated in Figure 23b at 15 μm, the maximum SRF requires convolution out to 17 full-widths-half-maximum (FWHM) to yield convolution errors < 0.1K. To achieve a comparable brightness temperature error at 15 μm with the minimum SRF requires convolution out to only 10 FWHM, 23c. In comparison, convolution out to 17 FWHM at 4 μm with the minimum SRF and 23 FWHM with the maximum SRF, Figure 24b and c, respectively, gives brightness temperature errors ~ 0.25K. To achieve an error of 0.1K at 4 $\mu m$with the minimum SRF requires convolution to at least 23 FWHM.

It is expected the channel center frequencies may drift by several percent of the FWHM when in orbit. In addition, a larger shift may occur during launch. Simulations show that the observed radiances can be interpolated to a fixed grid of channel centers for small offsets on

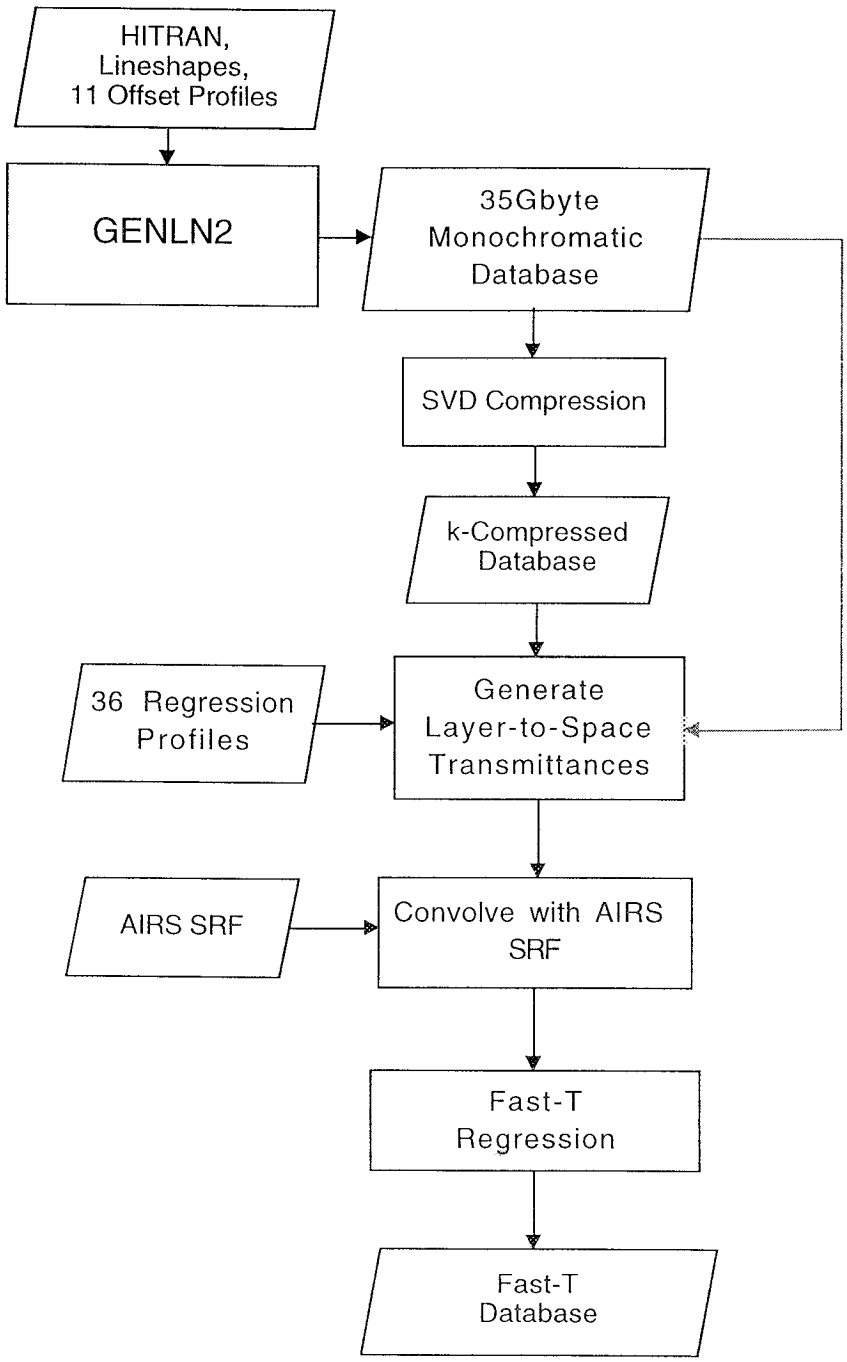

Figure 15: Flowchart for generation of the fast forward algorithm.

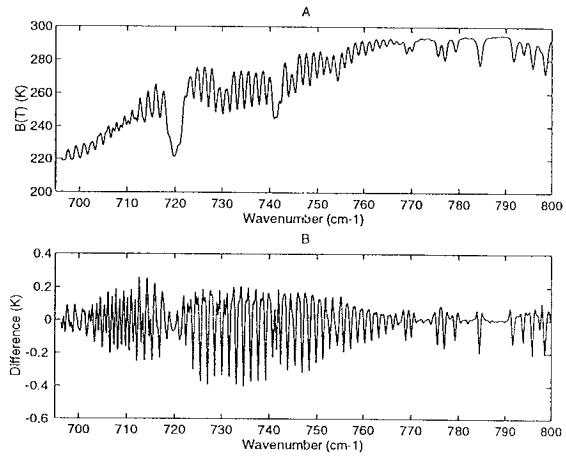

Figure 16: (a) Partial AIRS spectrum in the 15 μm CO_2 band. (b) Brightness temperature error due to a 2% error in AIRS spectral resolution.

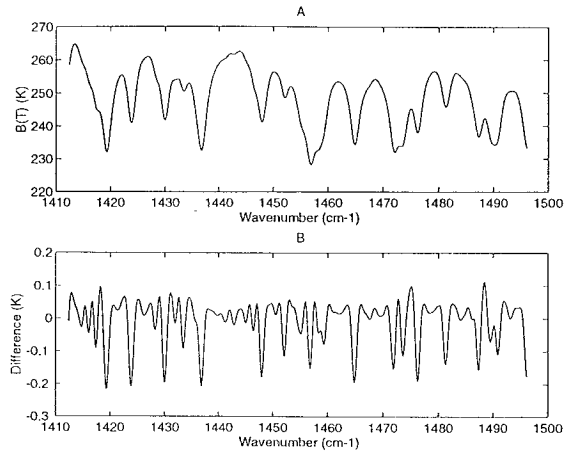

Figure 17: (a) Partial AIRS spectrum in the 7 μm H_2O band. (b) Brightness temperature error due to a 2% error in AIRS spectral resolution.

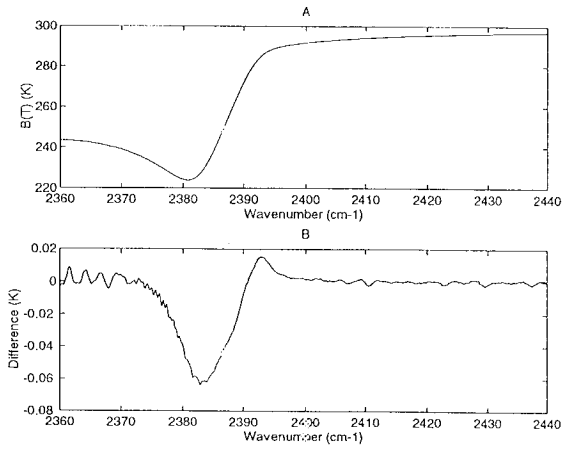

Figure 18: (a) Partial AIRS spectrum in the 4 μm CO_2 band. (b) Brightness temperature error due to a 2% error in AIRS spectral resolution.

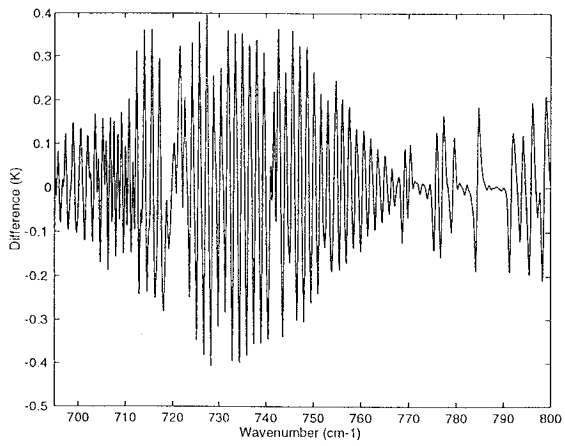

Figure 19: Brightness temperature error in the 15 μm CO_2 band due to a 1% shift in the AIRS channel center frequency .

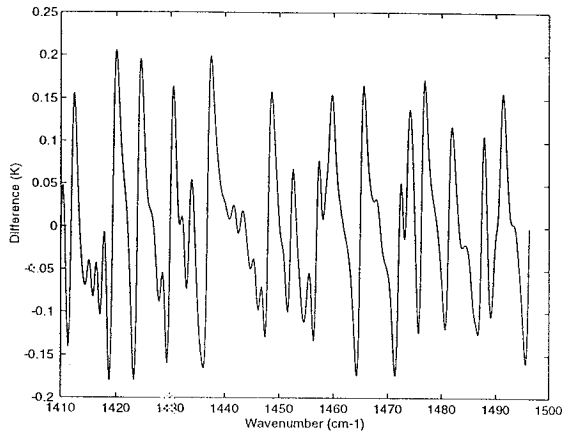

Figure 20: Brightness temperature error in the 7 μm H_2O band due to a 1% shift in the AIRS channel center frequency.

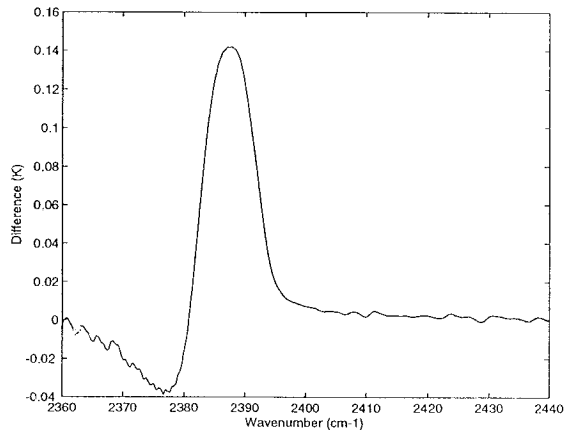

Figure 21: Brightness temperature error in the 4 μm CO_2 band due to a 1% shift in the AIRS channel center frequency.

the order of 5-10% of the FWHM. Consequently, once the in-orbit nominal channel centers have been determined, forward model coefficients for these channel centers will be generated and used in the retrievals. Remaining small drifts of the channel centers will be accounted for by interpolating the observed radiances to these fixed channel centers.

8 Validation of Forward Model and Fast Transmittance Algorithm

Validation of the forward model, as well as validation of improvements to the spectroscopy in the line-by-line radiative transfer codes, will require intensive field experiments utilizing a variety of instruments. These instruments include, but are not limited to, ground-based and aircraft LIDAR, ground-based and aircraft infrared spectrometers/interferometers, radiosondes (standard and any improved versions), and other instruments to perform *in situ* measurements of trace gases (H_2O, CO, O_3, *etc.*).

As previously mentioned, persistent differences between HIS observations and calculations due to H_2O emission at pressures < 500 mbar are a topic of concern. Given the difficulties already encountered in past field experiments to achieve the necessary co-location of remote spectra (*i.e.* HIS) and accurate radiosonde profiles of H_2O, every effort should be made for AIRS validation experiments to use the most advanced instruments for making *in situ* H_2Omeasurements. One possible field experiment to assist in bringing this problem to closure would be to fly both the HIS and a H_2O LIDAR on the ER-2 at the same time.

Another area of concern is the uncertainty in the cross-over point between domination of the continuum by self-broadening versus foreign-broadening. This cross-over takes place at

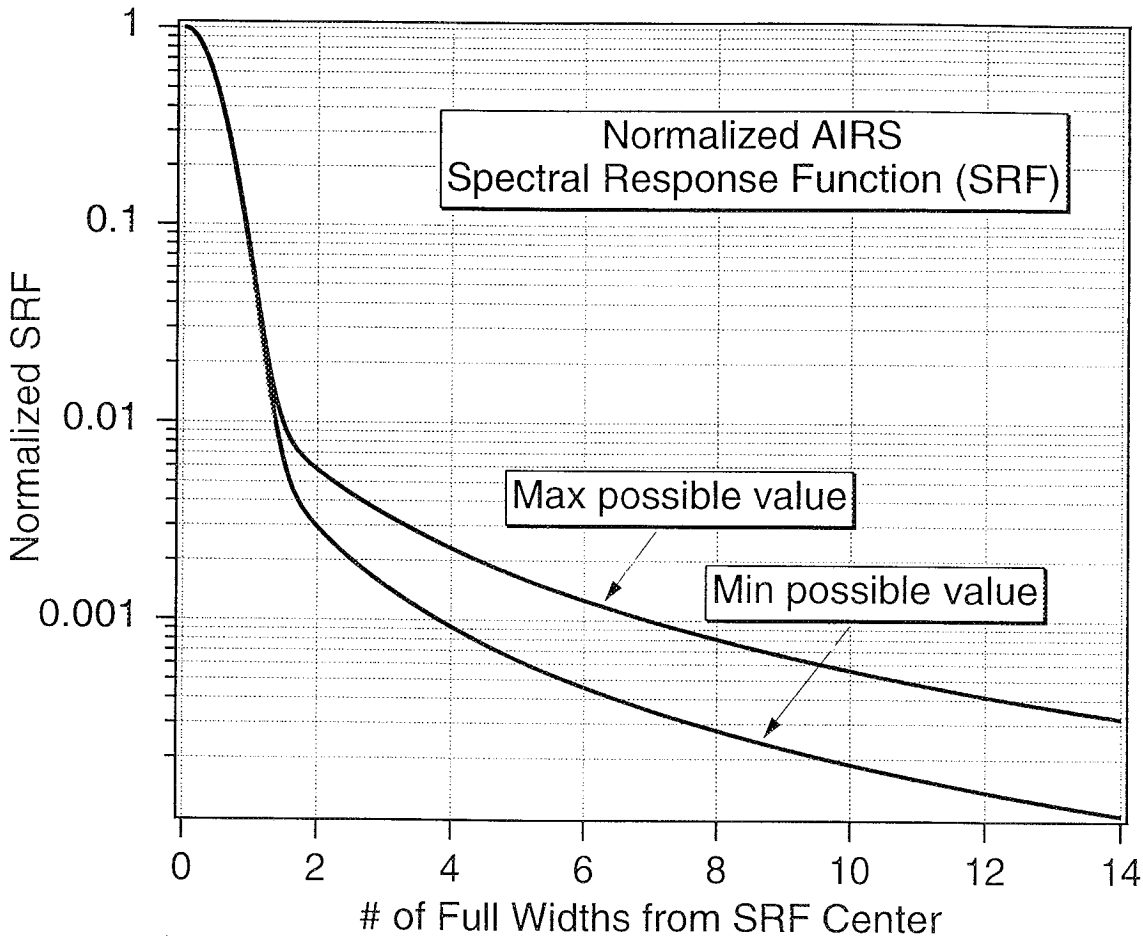

Figure 22: Old and New AIRS spectral response functions (SRF's) are plotted. The old SRF was used in the current AIRS forward model. The new SRF is shown for two channels, the first and last, to illustrate the range of differences in the far wing portion of the SRF.

wavenumber regions important for lower troposphere humidity sounding, somewhere in the edge of the 6 μm H_2O band. This cross-over point will be profile dependent, and is troublesome since the self-broadened continuum is quadratically dependent on H_2O amount while the foreign-broadened continuum depends linearly on H_2O amount.

In addition to validation experiments once AIRS is in orbit, validation experiments prior to the launch of AIRS would be invaluable for validation of recently derived spectroscopic improvements.

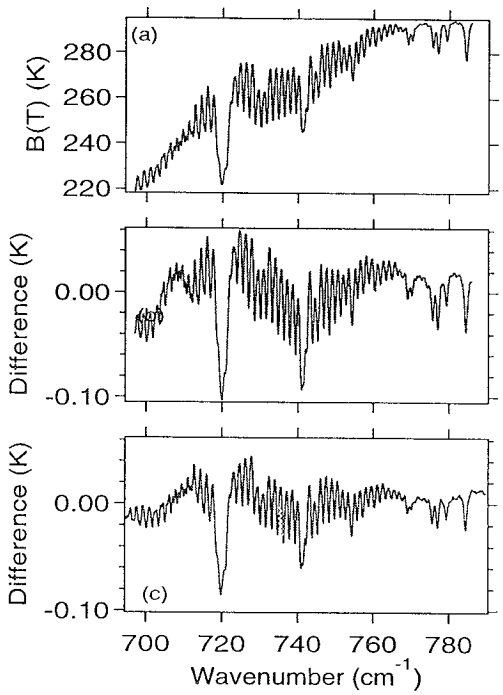

Figure 23: (a) Mean AIRS spectrum at 15 μm. (b) Mean brightness temperature errors from convolving out to 17 full-width-half-maximums (FWHM) with the maximum SRF shown in Figure 22. (c) Mean brightness temperature errors from convolving out to 10 full-width-half-maximums (FWHM) with the minimum SRF shown in Figure 22

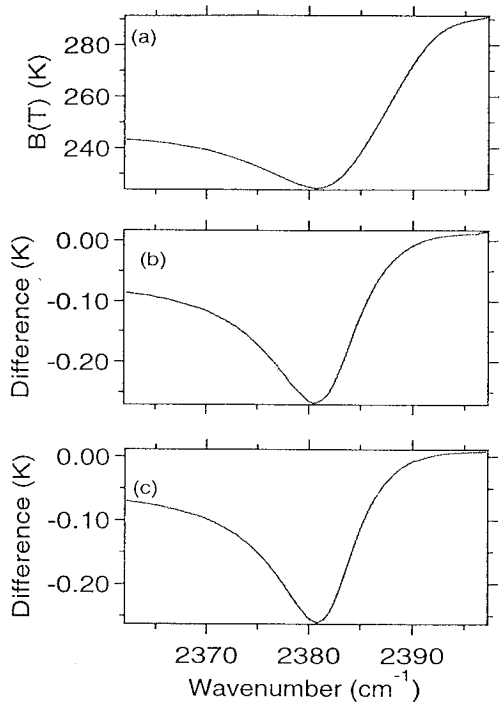

Figure 24: (a) Mean AIRS spectrum at 4 μm. (b) Mean brightness temperature errors from convolving out to 17 full-width-half-maximums (FWHM) with the maximum SRF shown in Figure 22. (c) Mean brightness temperature errors from convolving out to 17 full-width-half-maximums (FWHM) with the minimum SRF shown in Figure 22

References

[1] L.M. McMillin and H.E. Fleming. Atmospheric transmittance of an absorbing gas: a computationally fast and accurate transmittance model for absorbing gases with constant mixing ratios in inhomogeneous atmospheres. *Appl. Opt.*, 15(2):358-363, 1976.

[2] H. F. Fleming and L. M McMillin. Atmospheric transmittance of an absorbing gas 2. *Appl. Opt.*, 16:1366, 1977.

[3] L.M. McMillin and H.E. Fleming. Atmospheric transmittance of an absorbing gas. 2: A computationally fast and accurate transmittance model for slant paths at different zenith angles. *Appl. Opt.*, 16(5):1366-1370, 1977.

[4] L.M. McMillin, H.E. Fleming, and M.L. Hill. Atmospheric transmittance of an absorbing gas. 3: A computationally fast and accurate transmittance model for absorbing gases with variable mixing ratios. *Appl. Opt.*, 18(10):1600-1606, 1979.

[5] L. M. McMillin, L. J. Crone, M. D. Goldberg, and T. J. Kleespies. Atmospheric transmittance of an absorbing gas 4. *Appl. Opt.*, 34:6274, 1995.

[6] L. M. McMillin, L. J. Crone, and T. J. Kleespies. Atmospheric transmittance of an absorbing gas 5. *Appl. Opt.*, 34:8396, 1995.

[7] J.R. Eyre and H.M. Woolf. Transmittance of atmospheric gases in the microwave region: a fast model. *Appl. Opt.*, 27(15):3244-3249, 1988.

[8] J. Susskind, J. Rosenfield, and D. Reuter. An accurate radiative transfer model for use in the direct physical inversion of hirs2 and msu temperature sounding data. *J.Geophys.Res.*, 88(C13):8550-8568, 1983.

[9] Scott Hannon, L. Larrabee Strow, and W. Wallace McMillan. Atmospheric infrared fast transmittance models: A comparison of two approaches. In *Proceedings of SPIE Conference 2830, Optical Spectroscopic Techniques and Instrumentation for Atmospheric and Space Research II*, 1996.

[10] L. S. Rothman, R. R. Gamache, R. H. Tipping, C. P. Rinsland, M. A. H. Smith, D. C Benner, V. M. Devi, J. M. Flaud, C. Camy-Peyret, A. Perrin, A. Goldman, S. T. Massie, L. R. Brown, and R. A. Toth. The HITRAN molecular database: Editions of 1991 and 1992. *J. Quant. Spectrosc. Rad. Trans.*, 48:469-507, 1992.

[11] R. A. Toth. private communication, 10/13/94. self-broadened H_2O widths, 1994.

[12] R. A. Toth. private communication, 12/06/94. Air- and N_2-broadened H_2O widths, 1994.

[13] L. L. Strow. The measurement of global carbon monoxide using the Atmospheric InfraRed Sounder (AIRS). In A. Chedin, M.T. Chahine, and N.A. Scott, editors, *High Spectral Resolution Infrared Remote Sensing for Earth's Weather and Climate Studies*, pages 351–362. Berlin: Springer Verlag, 1993.

[14] L. L. Strow, D. C. Tobin, and S. E. Hannon. A compilation of first-order line-mixing coefficients for CO_2 Q-branches. *J. Quant. Spectrosc. Rad. Trans.*, 52:281, 1994.

[15] D. C. Tobin. Carbon dioxide lineshapes in $\Pi \leftarrow \Sigma$ and $\Pi \leftarrow \Delta$ vibrational transitions. Master's thesis, University of Maryland Baltimore County, 1993.

[16] D. C. Tobin. *Infrared Spectral Lineshapes of Water Vapor and Carbon Dioxide.* PhD thesis, University of Maryland Baltimore County, 1996.

[17] Curtis P. Rinsland and L. Larrabee Strow. Line mixing effects in solar occultation spectra of the lower stratosphere: measurements and comparisons with calculations for the 1932 cm^{-1} Q branch. *Appl. Opt.*, 28:457, 1989.

[18] David P. Edwards and L. Larrabee Strow. Spectral line shape considerations for limb temperature sounders. *J. Geophys. Res.*, 96:20,859–20,868, 1991.

[19] C. Cousin, R. Le Doucen, C. Boulet, and A. Henry. Temperature dependence of the absorption in the region beyond the 4.3μm band head of CO_2: 2: N_2 and O_2 broadening. *Appl. Opt.*, 24:3899, 1985.

[20] L. L. Strow, D. C. Tobin, and S. E. Hannon, 1996. in preparation.

[21] D.E. Burch and D.A. Gryvnak. Continuum absorption by water vapour in the infrared and millimeter regions. In A. Deepak, T.D. Wilkerson, and L.H. Rhunke, editors, *Atmospheric water vapour*, pages 47–76. Academic Press, NY, 1980.

[22] D. E. Burch. Continuum absorption by H_2O. Technical Report AFGL-TR-81-0300, AFGL, 1982.

[23] D. E. Burch and R. L. Alt. Continuum absorption by H_2O in the 700-1200 cm^{-1} and 2400-2800 cm^{-1} windows. Technical Report AFGL-TR-84-0128, AFGL, 1984.

[24] D. E. Burch. Absorption by H_2O in narrow windows between 3000 and 4200 cm^{-1}. Technical Report AFGL-TR-85-0036, AFGL, 1985.

[25] S. A. Clough. The water vapor continuum and its role in remote sensing. In *Optical Remote Sensing of the Atmosphere*, Salt Lake City, UT, February 1995.

[26] D. C. Tobin, L. L. Strow, W. J. Lafferty, and Wm. B. Wm. Olson. Experimental investigation of the self- and N_2- broadened continuum within the ν_2 band of water vapor. *Appl. Opt.*, 35:1, 1996.

[27] 1995. Burch's measurements have been modified to be consistent with the local lineshape definition used here and were kindly provided by Clough, S. A.

[28] D.P. Edwards. Genln2: A general line-by-line atmospheric transmittance and radiance model. NCAR Technical Note 367+STR, National Center for Atmospheric Research, 1992.

[29] L. Larrabee Strow, Robert G. Benson, and Scott E. Hannon. Computation of monochromatic infrared atmospheric transmittances using compressed look-up tables. In *Proceedings of SPIE Conference 2830, Optical Spectroscopic Techniques and Instrumentation for Atmospheric and Space Research II*, 1996.